INSTITUTE OF PHYSICS PUBLISHING JOURNAL OF MICROMECHANICS AND MICROENGINEERING

J. Micromech. Microeng. **16** (2006) 1571–1578 doi:10.1088/0960-1317/16/8/018

Creating micro-scale surface topology to achieve anisotropic wettability on an aluminum surface

Andrew D Sommers and Anthony M Jacobi

Department of Mechanical and Industrial Engineering,
University of Illinois at Urbana-Champaign, Urbana, IL, USA

E-mail: asommers@uiuc.edu and a-jacobi@uiuc.edu

Received 30 March 2006, in final form 17 May 2006
Published 29 June 2006
Online at stacks.iop.org/JMM/16/1571

Abstract

A technique for fabricating micropatterned aluminum surfaces with parallel grooves 30 μm wide and tens of microns in depth is described. Standard photolithographic techniques are used to obtain this precise surface-feature patterning. Positive photoresists, S1813 and AZ4620, are selected to mask the surface, and a mixture of BCl_3 and Cl_2 gases is used to perform the etching. Experimental data show that a droplet placed on the micro-grooved aluminum surface using a micro-syringe exhibits an increased apparent contact angle, and for droplets condensed on these etched surfaces, more than a 50% reduction in the volume needed for the onset of droplet sliding is manifest. No chemical surface treatment is necessary to achieve this water repellency; it is accomplished solely by an anisotropic surface morphology that manipulates droplet geometry and creates and exploits discontinuities in the three-phase contact line. These micro-structured surfaces are proposed for use in a broad range of air-cooling applications, where the management of condensate and defrost liquid on the heat transfer surface is essential to the energy-efficient operation of the machine.

(Some figures in this article are in colour only in the electronic version)

1. Introduction

In a broad range of air-cooling applications, water retention on the air-side surface of metallic heat exchangers is problematic because it can reduce the air-side heat transfer coefficient, increase core pressure drop and provide a site for biological activity. In refrigeration systems, the accumulation of frost on metallic fins requires periodic defrosting and results in an energy expenditure. When water is retained on these surfaces following the defrost cycle, ice is more readily formed in the subsequent cooling period, and such ice can lead to shorter operation times before the next defrost is required. Many microelectromechanical systems (MEMS) also actively use, or passively rely upon, liquid–surface interactions. Examples include the lubrication of MEMS motors and the delivery of ink in inkjet printers. When operating in humid environments, the condensation of water onto MEMS devices is especially problematic since water retention can cause moving parts to stick and decrease the overall heat transfer performance of the device. Thus the management and control of liquid water droplets on a variety of surfaces, especially metal substrates, is vital to energy efficiency, functionality and maintenance.

Very few papers have been published on the hydrophobizing of metal substrates, and most attempts to create hydrophobic metal surfaces have involved wet chemistry techniques or coatings. Studies concerned with the manufacture of hydrophobic aluminum surfaces are especially rare in the literature. The authors were unable to locate any article in the open literature reporting the exclusive use of surface topography to hydrophobize an aluminum surface. Shirtcliffe *et al* [1] studied patterned copper surfaces produced using wet chemistry and separately using electrodeposition. Both surfaces, however, were hydrophobized using a fluorocarbon wash. Shibuichi *et al* [2] described a wet chemistry technique utilizing H_2SO_4 and a silane coupling reagent to create a fractal-structured, water-

repellant surface through anodic oxidation. Contact angles as high as 160° were reported. However, the contact angles were measured for droplets of a water–methanol mixture, and this fractal-surface method produced surface cracks and small spherical holes that might be problematic in applications with thermal cycling (i.e. under frosting/defrosting conditions).

Using a Beck's dislocation etchant (i.e. a mixture of HCl, H_2O and HF), Qian and Shen [3] were able to preferentially dissolve dislocation sites in a polycrystalline aluminum sheet, creating a labyrinth of rectangular pits on the surface. Contact angles larger than 150° were reported. However, this method also required subsequent treatment of the surface with fluoroalkysilanes.

Bayiati *et al* [4] focused on the selective deposition of fluorocarbon (FC) films on metal surfaces, specifically aluminum, over SiO_2 surfaces in an effort to control surface wettability. For this study, C_4F_8, CHF_3 and CHF_3/CH_4 fluorocarbon gases were selected and plasma parameters were varied to achieve optimal deposition selectivity. Hydrophobic surface properties were achieved on aluminum. However, the maximum achievable water contact angle using this method was 118°, and water droplets deposited on the modified aluminum surfaces for long times were observed to penetrate the film and spread on the surface as if it were hydrophilic.

In a related paper on fluorocarbon coatings, Ji *et al* [5] were able to deposit hydrophobic multilayer CF_x coatings on aluminum using a benign $Ar/C_2H_2/C_3F_8$ chemistry in a sputtering/plasma-enhanced chemical vapor deposition system. The degree of hydrophobicity was observed to depend both on the fluorine content of the coating and the surface morphology. However, because of problems with adhesion on aluminum, a chromium intermediate layer had to be deposited onto the aluminum substrate before the CF_x coating could be deposited. Furthermore, the maximum advancing angle achieved using this method was only 105°.

In a paper with deicing applications, Somlo and Gupta [6] prepared a weakly hydrophobic 6061 aluminum alloy surface through a dipping process involving dimethyl-*n*-octadecilcholorosilane (DMOCS) and studied the tensile strength of the ice/DMOCS interface. The DMOCS coating had the lowest ice adhesion strength of all tested surface treatments. However, no contact angle information was provided, and the adherence and longevity of the DMOCS coating were not quantified.

The literature is replete with articles concerning parallel groove geometries and their effect on wettability. Overwhelmingly, these articles have focused on silicon substrates and qualitative observations of water droplets. Due to their abundance, only the most germane works will be discussed. Morita *et al* [7] offered insight into the anisotropic wetting behavior of micropatterned fluoroalkylsilane monolayer surfaces with alternating hydrophilic/hydrophobic lines of width 1–20 μm. For all line widths, they observed that the static and dynamic contact angles of a droplet oriented orthogonally to the stripes were 10–30° larger than those of the droplet oriented parallel to the stripes. Unlike earlier researchers, Morita and co-workers suggested that the source of this anisotropy is neither the line tension nor the asperity but the energy barrier to wetting. In the orthogonal direction, this energy barrier is the hydrophobic region and therefore periodic. In the parallel direction, however, there is no periodic energy barrier to wetting and the droplet is allowed to advance continuously. No general model explaining contact angle variation or drop adhesion was offered.

Yoshimitsu *et al* [8] studied the sliding behavior and contact angle variation of water droplets on hydrophobic pillar and groove structures prepared from a silicon wafer by dicing it and coating it with fluoroalkylsilane. They found that the sliding angle of the water droplet was smallest for the grooves in a direction parallel to gravity, followed by the pillar structure and then the grooves in an orthogonal direction. Although the contact angle was lower on the groove structure, the groove structure exhibited better water-shedding characteristics in the parallel direction than the pillar structure because of its low energy barrier to the movement of the contact line. This observation showed that a reduction in the solid–water contact area without regard to the contact line may not impart better sliding behavior.

Chen *et al* [9] examined the apparent contact angle and shape of water droplets on parallel-grooved surfaces using both numerical and experimental approaches. They found that multiple equilibrium shapes were possible, and the final predicted shape depended largely on the number of channels on which the drop resided. Their numerical model was compared to contact angle measurements of water droplets on a PDMS substrate having a pillar width of 23 μm, groove width of 25.6 μm and a pillar height of 30 μm. The apparent contact angle viewed along the channels was typically larger than the contact angle viewed perpendicular to the channels. This behavior, attributed to the pinning of the droplet against the pillars, was observed both numerically and experimentally. In their work, however, Chen *et al* examined very small water droplets (i.e. 0.59–5.7 μL) and did not provide the contact angle as a function of the azimuthal angle.

The only paper located that treats condensation of water vapor onto a superhydrophobic grooved surface is the work of Narhe and Beysens [10]. In this work, silicon substrates were prepared using the same technique outlined by Yoshimitsu [8] and treated by silanization. The contact angles were 130° and 110° in the directions orthogonal and parallel to the grooves, respectively. Four stages of droplet growth were identified: initial, intermediate, drying and large drop formation. During the drying stage, the instantaneous drying of the top surface of the grooves was observed due to the coalescence of water droplets with completely filled channels. For long times, bridges formed between the channels resulting in large droplets that covered several grooves. This work, however, exclusively focused on condensation and not the liquid from a melting frost layer.

In summary, there has been considerable research aimed at manufacturing and understanding hydrophobic surfaces. However, only a very small subset of that research has involved metallic substrates. Most attempts to impart hydrophobic characteristics to a surface have focused not only on surface geometry but also on the modification of the surface energy by chemical treatment. Overwhelmingly, these papers have focused on silicon and polymer substrates, and the technical literature is replete with articles describing micro-size etching techniques for silicon. However, silicon is not suited for the

air-cooling applications motivating this study, and the authors are aware of only a few papers that specifically address the fabrication of a hydrophobic aluminum surface. Furthermore, thermal cycling in air-cooling systems and the accompanying cyclical condensation, freezing, melting and draining of water on these aluminum surfaces raises concerns regarding robustness and longevity of a coating-based approach for the manipulation of wettability in application.

In this paper, we report a method for fabricating controlled micro-scale, anisotropic topological features on aluminum surfaces for the purpose of exploiting those features to affect the surface wettability. Micro-scale grooves are studied because they can be made in mass production and might provide directional wettability or wettability gradients useful for causing water to drain from a surface. Aluminum is studied because it is naturally hydrophilic and is widely used in heat and mass transfer applications, because of its low cost and excellent mechanical and thermal properties.

2. Experimental methodology

The specific contact angle that a water droplet forms on a surface has long been used as a gauge of the hydrophobicity of the surface. However, depending on how the water droplet forms on the surface, at least two different wetting regimes can exist. The first type known as the 'wetted surface' forms when the water droplet completely fills the surface asperities. This particular wetting regime, which may result from melting frost or condensing water vapor, is usually described by Wenzel's theory of wetting [11]. The second type known as the 'composite surface' occurs when the droplet is suspended over the asperities, leaving air trapped beneath it. This form of wetting frequently occurs when the droplet is injected by syringe onto a surface having sufficiently small surface features. 'Composite surfaces' are described by Cassie's theory of wetting [12]. By themselves, the large contact angles associated with a hydrophobic surface do not ensure that a surface easily sheds water. Therefore, the sliding angle is a useful criterion when evaluating the water drainage behavior of surfaces. The sliding angle is the critical angle for a water droplet of known mass to first begin sliding down an inclined surface. In this paper, both wetted and composite surfaces are explored, and sliding angle data are presented.

2.1. Surface fabrication

Parallel channels approximately 30 μm wide and running the length of the surface were etched into plates of aluminum alloy 1100 (99.9% pure Al), 63.5 mm by 63.5 mm by 3.2 mm in size. The fronts of the plates were machine buffed to ensure good surface reflectivity, with care taken to ensure that they remained optically flat. On the backs of the plates, two holes were drilled to a depth of approximately 2.5 mm and threaded to allow for backside mounting to a Peltier cooling stage. Additionally, eight holes of varying depth were drilled into the sides of the plates, four on each side, to accommodate the insertion of thermocouples for surface temperature monitoring (see figure 1). Before polishing, the plates had an average roughness, R_a, of 350 nm, whereas after polishing the R_a was 25–35 nm.

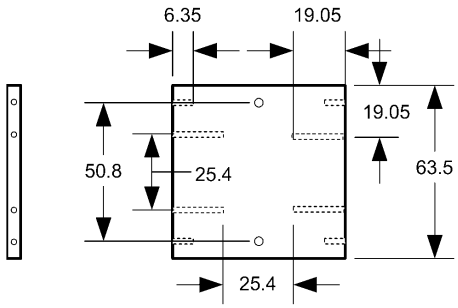

Figure 1. Test specimens were constructed from aluminum alloy 1100 and etched to have 30 μm wide, parallel channels running the length of the plate. Ports were drilled into the sides of the plate to allow for the insertion of thermocouples. Dimensions shown are in mm.

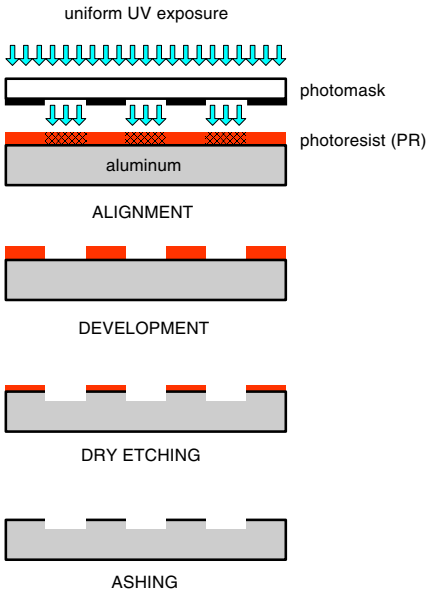

Figure 2. Standard photolithography and wet chemistry techniques were used to pattern photoresist on the aluminum plate prior to etching.

Standard photolithographic practices were employed in preparing the plates for etching (see figure 2). First, one of two different photoresists was spin coated onto the aluminum surface using a Headway spinner. The choice of photoresist was made on the basis of the etch selectivity of the photoresist, the thickness of the photoresist layer after spinning and the relative ease of removing the photoresist following etching. For shallower etches (i.e. $\leqslant$5 μm), positive photoresist S1813 was used; while for the deeper etches (i.e. $>$5 μm), AZ4620 positive photoresist was chosen. In all cases, the surface of the aluminum was cleaned with acetone, rinsed with isopropyl alcohol and dried using a stream of nitrogen gas prior to spinning. Because the process differed for the two photoresists, the procedural details are summarized in table 1. After the photoresist was spun onto the substrate, the aluminum plate was soft baked to prevent mask sticking. A Quintel Q7000 IR backside mask aligner was then used to align the mask over the aluminum substrate and expose the photoresist to UV light. The photomask was made of soda lime and coated with chrome and was 127 $\times$ 127 mm

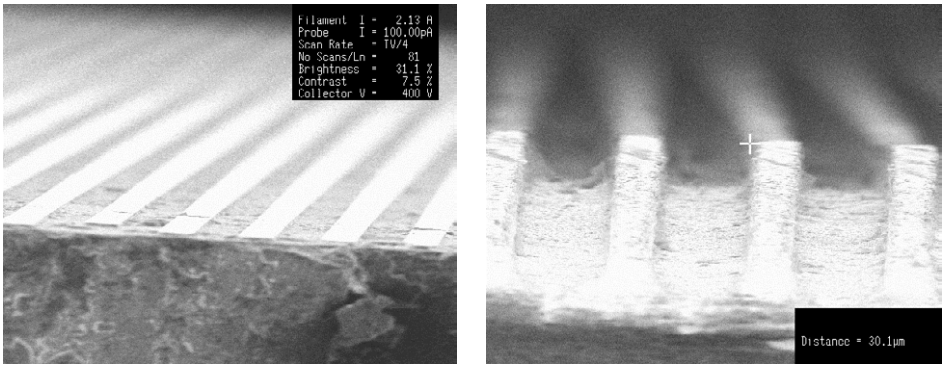

Figure 3. SEM images of sample 1 with an etch depth of 5.2 μm (shown on left) and sample 3 with an etch depth of 27.0 μm (shown on right).

Table 1. Photoresist experimental test matrix.

Sample no./ photoresist (PR)	Spinning	Soft bake	Exposure	Developer	Post bake	PR thickness
1 S1813	25 s at 4000 rpm	110 °C 1 min	9.4 mW cm^{-2} 11 s	CD-30 60 s	125 °C 2 min	∼1.9 μm
2 AZ4620	30 s at 2000 rpm	65 °C → 100 °C 20 min ramp	9.4 mW cm^{-2} 60 s	AZ 400 K, 1:4 3 min	110 °C → 140 °C 20 min ramp	∼12.0 μm
3 AZ4620	30 s at 2000 rpm	65 °C → 100 °C 20 min ramp	9.4 mW cm^{-2} 60 s	AZ 400 K, 1:4 3 min	110 °C → 140 °C 20 min ramp	∼12.0 μm

in size. Development was by immersion and agitation in a beaker. Each of the samples was then inserted into a TI Planar Plasma Etch system and subjected to a 300 W oxygen plasma for 20 s for residual photoresist removal. The samples were then post-baked to completely harden the masking layer and transferred to the PlasmaTherm SLR-770 inductively coupled plasma reactive ion etcher (ICP RIE) for dry chemical etching. Afterward, the samples were rinsed with copious amounts of acetone and gently brushed with a swab to remove the photoresist layer. The TI Planar Plasma Etch system was then used again in an ashing step to remove any remaining organic material on the surface by means of an oxygen plasma at 600 W for 5 min.

The actual dry chemical etching was performed in three steps. First, the native oxide layer was removed via a 1 min surface scavenging process involving 20 sccm of BCl_3 at a power setting of 30 W to electrode RF1 and 300 W to electrode RF2. The bias generated by the plasma was approximately 150 VDC. The next step was the main etch. A mixture of 20 sccm BCl_3 and 5 sccm Cl_2 was fed to the chamber at a setting of 12 W to RF1 and 300 W to RF2. The bias induced in this step was 77–80 VDC. Three different samples were made with only the etch time being varied. Sample 1 required an etch time of 33 min, sample 2 was etched for 99 min, and sample 3 was etched for 200 min. Following this procedure, a short passivation step was performed to stop the etching. A 1 min 20 sccm O_2 plasma at 50 W RF1, 300 W RF2 was used for the passivation. The samples were then removed, and each sample was analyzed using a Cambridge S-360 scanning electron microscope and an Alpha-Step profilometer to determine the surface geometry accurately. The final etch depths were 5.2 μm, 15.7 μm and 27.0 μm for samples 1, 2 and 3, respectively (see figure 3). In all cases, the channel spacing was fixed by the mask at approximately 30 μm; although for longer etch times, etching of the sidewalls was apparent. As a result, sample 1 had a final channel width of 33.2 μm; the channel width for sample 2 was 34.8 μm and sample 3 had a channel width of 36.8 μm. Thus, the etch rate (ER) for this recipe was approximately 0.11–0.16 μm min^{-1}.

2.2. Measurements in a composite-surface wetting mode

Information about the contact angle of water droplets injected onto these surfaces was obtained using a KAPPA DX 10-1394a high-resolution CCD camera. The camera was mounted opposite to a light source on an arm that could be rotated around a fixed plate containing the test surface and droplet. Two different configurations of the etched surface channel geometry relative to gravity were tested as shown in figure 4. In the 'parallel' orientation, the etched channels were aligned parallel to gravity, whereas in the 'perpendicular' orientation, the channels were oriented orthogonal to gravity. The sample and water droplet were placed inside a vapor-tight, transparent box to minimize the effect of evaporation on droplet geometry during image acquisition. Droplets in the range from 5 μL to 25 μL were injected onto the test surface using a micro-syringe, and the contact angle was measured from droplet profiles for azimuthal angles of 0°, 90° and 180°. Standard image analysis software was used to process the images and determine the contact angle and base dimensions of the droplet.

Determination of the critical inclination angle for sliding on these surfaces was accomplished using a tilt-table assembly with an extendable lever arm that permitted continuous

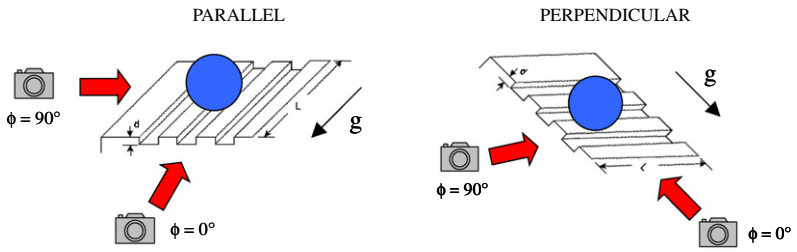

Figure 4. Two different contact angle measurement configurations were examined—one with channels oriented parallel to gravity (shown on left) and the other with channels oriented perpendicular to gravity (shown on right).

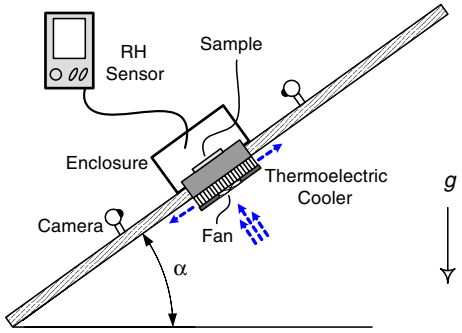

Figure 5. A Peltier stage was used to condense water on each sample within an enclosure. Individual droplets were permitted to grow and were then tested for their critical inclination angle.

inclination of the surface from horizontal. A droplet was placed on the test sample in the horizontal position using a micro-syringe, and the plate was then slowly tilted until imminent droplet motion was detected. A KAPPA DX 10-1394a high-resolution CCD camera was used to record profile images of the droplets from a location parallel to the base. This arrangement permitted optical droplet magnification of up to 25×. Prior to droplet injection, test images with grid marks were recorded for calibration purposes. Multiple measurements were recorded for each droplet volume which permitted the critical inclination angle and related droplet diameter to be checked for consistency. The maximum uncertainty in the measured contact angle was approximately 3° while the uncertainty in the critical inclination angle was only 1°. Typical uncertainty in drop diameter was 2–3% with the maximum uncertainty not exceeding 7%.

2.3. Measurements in a wetted-surface wetting mode

A platform equipped with a miniature testing chamber, shown in figure 5, was built to test the samples under condensing conditions. A thermoelectric cooler was used to condense water on these samples at a fixed surface temperature of approximately 3–5 °C and relative humidity of 70% ± 3%. The humidity was measured using a capacitive thin-film sensor, and moisture was provided by a cool-mist ultrasonic humidifier. The surface temperature was measured using a single type-T thermocouple in intimate contact with the sample on its side. Droplets were condensed onto the aluminum sample for a predetermined amount of time with the platform in the horizontal position (i.e. $\alpha = 0°$). Intermittently, a cotton swab was used to remove excess water from the surface to

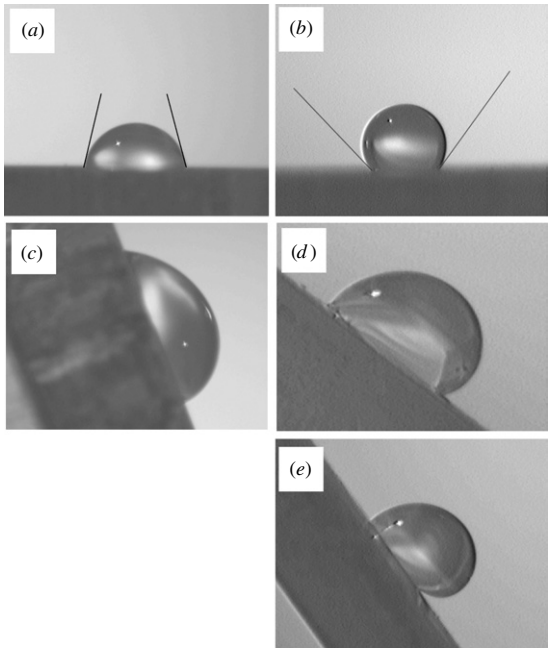

Figure 6. Droplet images on horizontal and inclined surfaces: (*a*) baseline—$\theta = 75°$; (*b*) sample 3 (parallel, $\phi = 0°$)—$\theta = 129°$; (*c*) baseline—$\theta_{adv} = 79°$, $\theta_{rec} = 60°$, $\alpha_{critical} = 69°$; (*d*) sample 2 (parallel)—$\theta_{adv} = 121°$, $\theta_{rec} = 84°$, $\alpha_{critical} = 38°$; and (*e*) sample 2 (perpendicular)—$\theta_{adv} = 153°$, $\theta_{rec} = 92°$, $\alpha_{critical} = 55°$.

allow for the undisturbed growth of single isolated droplets. Once a droplet of sufficient size was grown, the sample was transferred to the tilt-table assembly where the critical inclination angle was determined. The volume of the droplet was found by absorbing the droplet in a high-density filter paper after the critical condition was reached and weighing it on a Mettler AE 200 electronic balance accurate to ±0.0001 g. This method was compared against the volume found by two other techniques—numerical integration of data taken from droplet profile images and the actual extraction of the droplet into a micro-syringe. The agreement among the methods was found to be acceptable (i.e. error < 11% for $n = 10$).

3. Results and discussion

3.1. Contact angle data

The apparent contact angle of composite-surface water droplets placed on these etched samples by micro-syringe increased by as much as 54° as compared to the baseline

surface (see figures 6(*a*) and (*b*)) indicating an apparent increase in hydrophobicity. The contact angle of the baseline surface was 75°, while the contact angle of sample 3 in the parallel configuration was found to be approximately 129°. This change in wettability is best attributed to the discontinuities of the three-phase contact line and the pinning of the droplet by the groove structure. The regularly spaced grooves create a periodic change in the apparent surface energy encountered by the three-phase confluence as it moves perpendicular to the grooves. The increase in surface energy causes the contact line to be pinned at the edge of a groove until the groove can be bridged and the contact line advances in a stick-slip fashion. This pinning causes a preferential spreading parallel to the grooves. Droplet spreading is continuous in one direction but step-wise periodic in the other.

In figures 6(*c*)–(*e*), the advancing and receding contact angles are shown for 14 μL and 10 μL droplets on the baseline surface and sample 2, respectively. Droplet profiles were recorded for sample 2 in both the parallel and perpendicular configuration. Sample 2 exhibits larger contact angle hysteresis than the baseline sample. For the baseline surface, the measured advancing contact angle was 79°, while the receding contact angle was found to be 60°. For sample 2 in the parallel orientation, the advancing contact angle was 121°, and the receding contact angle was 84°. Contact angle hysteresis is the absolute difference between the advancing and receding contact angles and is often used as a gauge of hydrophobicity [13–17]. Therefore, one might expect sample 2 to have larger critical angles of inclination for sliding, α_c, than those of the baseline surface. However, the opposite was found to be true. Sample 2 had a critical inclination angle of only 38° when in the parallel orientation, but the baseline surface had a critical inclination angle of 69° for a slightly larger droplet. This observation points to the importance of the contact line and the profound effect that topology can have on the contact angle.

It was also observed that larger critical angles of inclination were manifested by sample 2 in the perpendicular configuration as compared to the parallel configuration. For identical droplet volumes and similar receding contact angles, the advancing contact angle was more than 30° larger for sample 2 in the perpendicular orientation. This observation supports the idea that these etched channels act as energy barriers to spreading.

3.2. Water retention data

The so-called critical droplet refers to a droplet large enough that the surface tension retaining force is equal to the gravitational drainage force and therefore occurs at the point of incipient motion. Understanding the shape and size of the critical droplet is the key to understanding the mechanisms of droplet retention on a surface. The critical droplet diameter, defined as the length of the major axis of the droplet at incipient motion, was found from droplet profile images. The critical diameter (and hence critical volume) for sliding of droplets forming a composite surface on sample 2 was reduced when compared to the baseline sample as shown in figure 7. In fact, an average reduction of 50% in the critical droplet diameter was observed for the case where the channels were

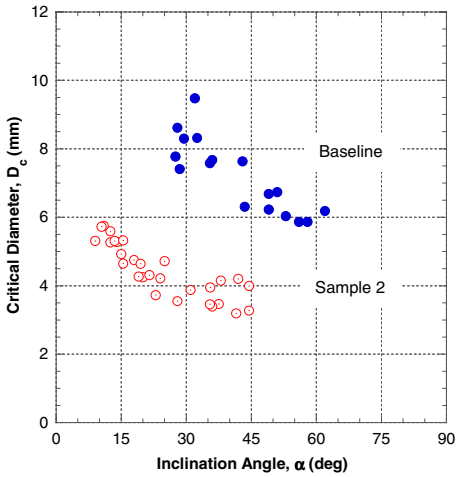

Figure 7. The maximum droplet diameter needed for sliding was reduced by approximately 50% for sample 2.

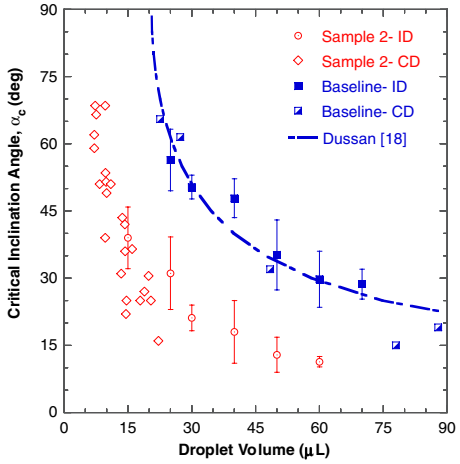

Figure 8. The reduction in the critical angle for sliding of sample 2 was manifest not only for injected droplets (ID) but also condensed droplets (CD).

oriented parallel to gravity. This reduced dependence on droplet mass for a large range of inclination angles further corroborates this idea that these etched surfaces serve to reduce the retentive force and can therefore assist in water removal. These critical droplet data, however, were specifically for the case of a composite surface, where the droplet is injected onto the surface through a micro-syringe. Because droplets in application typically wet the surface, additional data on wetted surfaces were obtained.

The condensing of water vapor on a surface follows a mode of droplet formation much different from droplet injection. Water fills the channels first and completely wets the surface, unlike injected droplet formation, in which some of the channels may remain dry. Shown below in figure 8 are critical inclination angle data for both injected droplets (ID) and condensed droplets (CD) on the two surfaces. For these data, the droplet volume of the injected droplets was determined by the micro-syringe, and the droplet volume of the condensed droplets was found by absorbing the droplet in high-density filter paper and then weighing it to determine

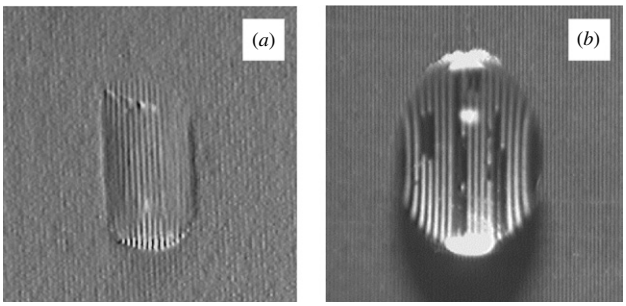

Figure 9. Frontal images of droplets on sample 2: (*a*) condensed droplets reveal a more elongated, parallel-sided shape, and (*b*) deposited droplets show evidence of both wetted and dry channels.

droplet mass. Similar critical angles for sliding were observed for injected droplets and condensed droplets on the baseline surface. Although the mechanisms of droplet formation are different, the absence of discernable roughness features on the baseline surface prevents a composite surface from being formed. As a result, injected droplets on the baseline surface behave similar to condensed droplets. The Dussan [18] equation derived for sessile droplets at the critical condition having only a small amount of contact angle hysteresis,

$$\left(\frac{\rho g \sin\alpha_c}{\gamma}\right)^{3/2} V = \left(\frac{96}{\pi}\right)^{1/2} \times \frac{(\cos\theta_{rec} - \cos\theta_{adv})^{3/2}(1+\cos\theta_{adv})^{3/4}\left(1-\frac{3}{2}\cos\theta_{adv}+\frac{1}{2}\cos^3\theta_{adv}\right)}{(\cos\theta_{adv}+2)^{3/2}(1-\cos\theta_{adv})^{9/4}}, \quad (1)$$

where ρ is the liquid density, γ is the surface tension of the liquid–vapor interface, V is the droplet volume, α_c is the critical inclination angle, θ_{adv} is the advancing contact angle and θ_{rec} is the receding contact angle, is also shown in figure 8. The Dussan [18] equation predicted the data well with only three required inputs, θ_{adv}, θ_{rec} and α_c, in addition to the fluid properties. Small differences, however, were observed between the condensed droplets and injected droplets on sample 2—namely, the critical inclination angle was reduced for the condensed droplets. These differences, believed to be due to the geometry of the three-phase contact line, were typically manifest for larger droplet volumes. The condensed droplets tended to be narrower and more elongated than the injected droplets as shown in figure 9, and as a result the length of their contact line opposing motion was shorter. Nonetheless, a consistent reduction of at least 50% in the critical droplet volume for sample 2 was observed.

This reduction in the retentive force is best understood by considering the discontinuities in the three-phase contact line and the base contour shape of the droplet. For droplets on the etched surface, the base contour shape is parallel sided. As a result, the surface tension force is orthogonal to the gravitational force on the sides of the droplet and does not contribute to the overall retention of the droplet. The discontinuities of the contact line at both the advancing and receding fronts also serve to reduce the surface tension force of the droplet, helping to minimize its retention. Thus, droplets on the etched samples can occupy additional surface area (and therefore volume) without the usual penalty of increased surface tension.

4. Conclusions

A method for creating controlled micro-scale, anisotropic topological features on aluminum surfaces has been presented, and the effects of these surface features on wetting and droplet retention have been quantified. This method of manipulating surface wettability relies solely on surface topology and does not require subsequent chemical treatment. The apparent contact angle for water droplets injected by syringe onto these etched surfaces was found to increase by as much as 54° for an etch depth of 27 μm, and lower overall critical angles of inclination were required for droplets to begin sliding on these surfaces. This drainage enhancement, observed for both injected droplets and condensed droplets, is due to the discontinuities in the three-phase contact line and the parallel-sided shape of the droplet base contour caused by the surface topology. The technique presented in this paper has broad applicability for metals other than aluminum, and its accompanying effect on wettability is of special relevance in air-cooling applications.

Acknowledgment

We are grateful for financial support from the Air Conditioning and Refrigeration Center (ACRC) at the University of Illinois.

References

[1] Shirtcliffe N J, McHale G, Newton M I and Perry C C 2005 Wetting and wetting transitions on copper-based super-hydrophobic surfaces *Langmuir* **21** 937–43
[2] Shibuichi S, Yamamoto T, Onda T and Tsujii K 1998 Super water- and oil-repellent surfaces resulting from fractal structure *J. Colloid Interface Sci.* **208** 287–94
[3] Qian B and Shen Z 2005 Fabrication of superhydrophobic surfaces by dislocation-selective chemical etching on aluminum, copper, and zinc substrates *Langmuir* **21** 9007–9
[4] Bayiati P, Tserepi A, Gogolides E and Misiakos K 2004 Selective plasma-induced deposition of fluorocarbon films on metal surfaces for actuation in microfluidics *J. Vac. Sci. Technol.* **22** 1546–51
[5] Ji H, Côté A, Koshel D, Terreault B, Abel G, Ducharme P, Ross G, Savoie S and Gagné M 2002 Hydrophobic fluorinated carbon coatings on silicate glaze and aluminum *Thin Solid Films* **405** 104–8
[6] Somlo B and Gupta V 2001 A hydrophobic self-assembled monolayer with improved adhesion to aluminum for deicing application *Mech. Mater.* **33** 471–80
[7] Morita M, Koga T, Otsuka H and Takahara A 2005 Macroscopic-wetting anisotropy on the line-patterned surface of fluoroalkylsilane monolayers *Langmuir* **21** 911–8
[8] Yoshimitsu Z, Nakajima A, Watanabe T and Hashimoto K 2002 Effects of surface structure on the hydrophobicity and sliding behavior of water droplets *Langmuir* **18** 5818–22
[9] Chen Y, He B, Lee J and Patankar N A 2004 Anisotropy in the wetting of rough surfaces *J. Colloid Interface Sci.* **281** 458–64
[10] Narhe R D and Beysens D A 2004 Nucleation and growth on a superhydrophobic grooved surface *Phys. Rev. Lett.* **93** 076103
[11] Wenzel T N 1936 Resistance of solid surfaces to wetting by water *Ind. Chem. Eng.* **28** 988–94
[12] Cassie A B D 1948 Contact angles *Discuss. Faraday Soc.* **3** 11–6

[13] Öner D and McCarthy T J 2000 Ultrahydrophobic surfaces: effects of topography length scales on wettability *Langmuir* **16** 7777–82
[14] Chen W, Fadeev A Y, Hsieh M C, Öner D, Youngblood J and McCarthy T J 1999 Ultrahydrophobic and ultralyophobic surfaces: some comments and examples *Langmuir* **15** 3395–99
[15] Jopp J, Grüll H and Yerushalmi-Rozen R 2004 Wetting behavior of water droplets on hydrophobic microtextures of comparable size *Langmuir* **20** 10015–9
[16] Fürstner R, Barthlott W, Neinhuis C and Walzel P 2005 Wetting and self-cleaning properties of artificial superhydrophobic surfaces *Langmuir* **21** 956–61
[17] Dussan V E B and Chow R T-P 1983 On the ability of drops or bubbles to stick to non-horizontal surfaces of solids *J. Fluid Mech.* **137** 1–29
[18] Dussan V E B 1985 On the ability of drops or bubbles to stick to non-horizontal surfaces of solids: Part 2. Small drops of bubbles having contact angles of arbitrary size *J. Fluid Mech.* **151** 1–20